Vector field controlled vortex lattice symmetry in LiFeAs using scanning tunneling microscopy

Songtian S. Zhang,[1,*] Jia-Xin Yin,[1,*,†] Guangyang Dai,[2] Hao Zheng,[1] Guoqing Chang,[1] Ilya Belopolski,[1] Xiancheng Wang,[2] Hsin Lin,[3] Ziqiang Wang,[4] Changqing Jin,[2] and M. Zahid Hasan[1,5,6,†]

[1]*Laboratory for Topological Quantum Matter and Spectroscopy (B7), Department of Physics, Princeton University, Princeton, New Jersey 08544, USA*

[2]*Institute of Physics, Chinese Academy of Sciences, Beijing 100190, China*

[3]*Institute of Physics, Academia Sinica, Taipei 11529, Taiwan*

[4]*Department of Physics, Boston College, Chestnut Hill, Massachusetts 02467, USA*

[5]*Lawrence Berkeley National Laboratory, Berkeley, California 94720, USA*

[6]*Princeton Institute for the Science and Technology of Materials, Princeton, New Jersey 08544, USA*

We utilize a combination of vector magnetic field and scanning tunneling microscopy to elucidate the three-dimensional field based electronic phase diagram of a correlated iron-based superconductor, LiFeAs. We observe, under a zero-field-cooled method, an ordered hexagonal vortex lattice ground state in contrast to the disordered lattice observed under a field-cooled method. It transforms to a fourfold-symmetric state by increasing the c-axis field and distorts elliptically upon tilting the field in-plane. The vortex lattice transformations correlate with the field-dependent superconducting gap that characterizes the Cooper pairing strength. The anisotropy of the vortex lattice agrees with the field-enhanced Bogoliubov quasiparticle scattering channel that is determined by the pairing symmetry in respect to its Fermi surface structure. Our systematic tuning of the vortex lattice symmetry and study of its correlation with Cooper pairing demonstrates the many-body interplay between the superconducting order parameter and emergent vortex matter.

Probing the response of correlated superconducting materials by varying composition, pressure, or magnetic field often reveals their emergent behavior intertwined with Cooper pairing [1,2]. The magnetic field response of their electronic structure is particularly noteworthy, as the magnetic flux can penetrate into superconductors and generate topological excitations of the superconducting order parameter—quantized vortices, whose quantum collective behavior in a correlated system remains elusive. Being a local probe with atomic resolution, scanning tunneling microscopy/spectroscopy (STM/S) has played a key role in imaging the vortices [1–4], while the impact of these topological defects on unconventional Cooper pairing has been much less explored due to technical challenges such as strong pinning, electronic/chemical inhomogeneity, or crystal quality factors [1–4]. STM studies on correlated superconductors have been largely limited to those with fields applied along fixed directions, which severely limits the exploration of the phase diagram and many-body vortex behavior. Here, we utilize a 0.4K-He3STM system coupled to a tunable 9 T–2 T–2 T vector field magnet to systematically manipulate the vortex lattice symmetry in superconducting LiFeAs and explore its interplay with the unconventional Cooper pairing.

LiFeAs is a remarkable superconductor in many respects. It is a stoichiometric, high $\kappa = \lambda/\xi \approx 50$, clean limit $l/\xi \approx 5$, strong-coupling superconductor [5–12] with a transition temperature $T_C \approx 17$ K (λ, ξ, and l are the penetration depth, coherence length, and mean-free path, respectively). We first research the behavior of the vortices over a large area on the sample with a 2 T field under both a zero-field-cooling (ZFC) and field-cooling (FC) process. We systematically uncover that the cooling process plays a critical role in selecting the ordering pattern of the vortex lattice. Under ZFC, the vortices form an ordered hexagonal lattice, in contrast to a disordered lattice reported previously in both STM and small-angle neutron-scattering studies [11,13], as demonstrated in the comparison of the fast Fourier transform (FFT) of the two maps in Figs. 1(a) and 1(b). The Delaunay triangulation analysis of the real-space vortices reveals that the ZFC technique predominately reduces the topological vortex defects, whose coordination numbers are not six. Further temperature-dependent measurement of the vortex lattice in Fig. 1(c) reveals a vortex thermal transition from order to disorder. The broad ringlike FFT signals for both ZFC and FC underline a highly disordered vortex (liquidlike) phase near T_C or H_{C2}. Based on the systematic evolution of the Bragg spots from the ringlike signal under ZFC and FC conditions, it is likely that the disordered vortices [Fig. 1(a)] are in a supercooled vortex liquid state [14], with its ground state as a vortex Bragg solid [Fig. 1(b)], likely due to LiFeAs being in the clean limit [11]. Physically, the ZFC has a much stronger perturbation to the vortex lattice, as vortices enter into the superconductor more violently, which could be the reason why the vortices can overcome the possible pinning and reach the ordered hexagonal lattice ground state.

Under this new ZFC condition, we gradually increase the c-axis field, transforming the hexagonal vortex lattice to a

---

*These authors contributed equally to this work.

†Corresponding authors: jiaxiny@princeton.edu; mzhasan@princeton.edu
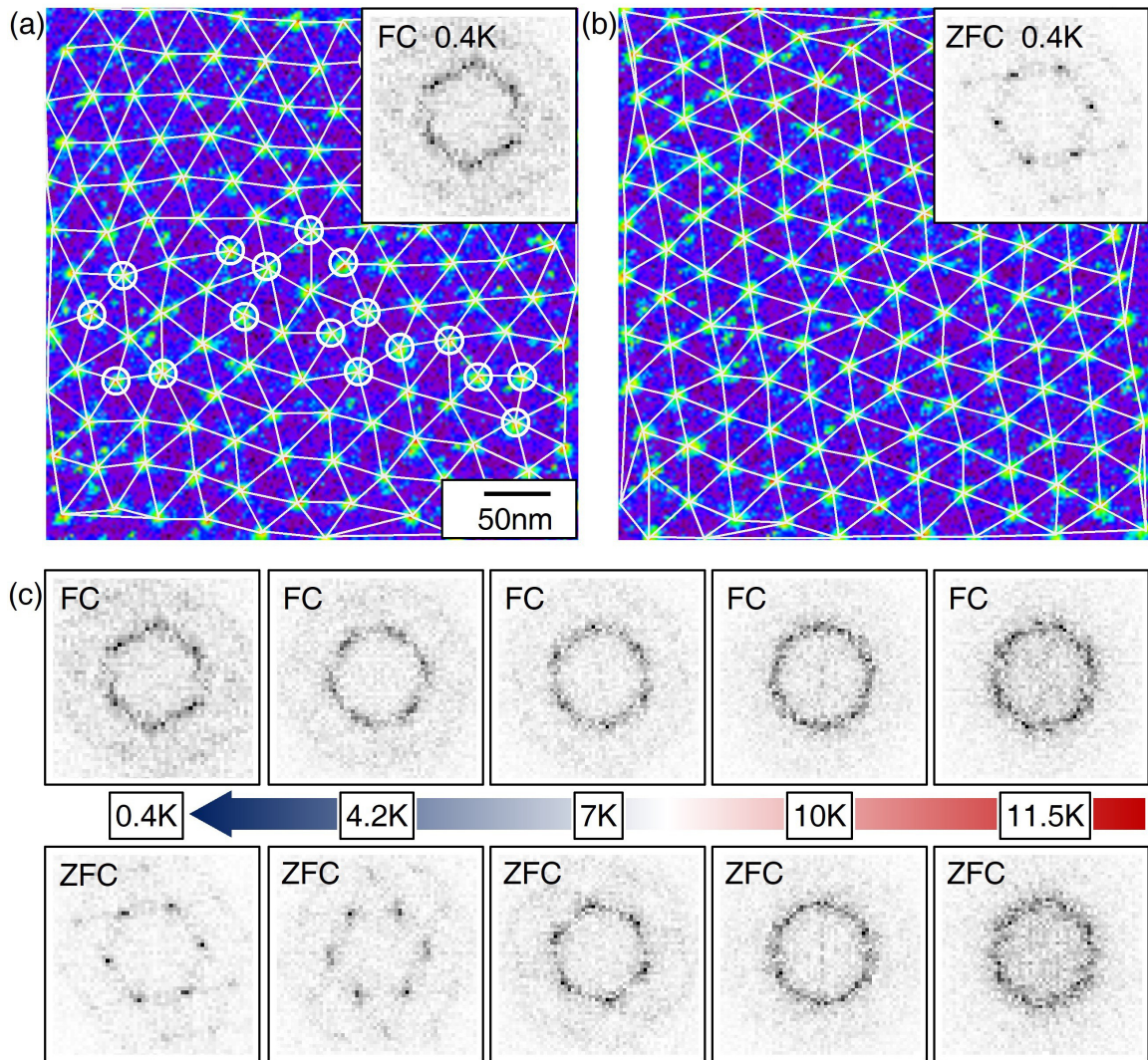
FIG. 1. (a),(b) The FC and ZFC zero-energy conductance maps measured for the same area, respectively. The white lines illustrate the Delaunay triangulation analysis. The open circles denote vortices whose coordination numbers are not 6. The inset shows the corresponding FFT image. (c) Temperature evolution of the FFT image with FC and ZFC techniques.

squarelike one [Fig. 2(a)]. The FFT of the maps shows that below 3 T, the vortices form a hexagonal lattice that is not strictly locked to the crystal lattice. Near 3 T, the hexagonal lattice transforms into an intermediate rhombuslike lattice with one axis locked to the crystal lattice. For fields of 4 T or higher, the vortices further form a quasisquare lattice with both axes locked to the Fe-Fe (100) lattice direction. This is in contrast to previous work performed under a FC process [11,13], which found moderately disordered lattices even at low fields, and the field-induced transition was consequently identified to result in a disordered amorphous phase. Furthermore, such a vortex transition does not seem to have been distinctly resolved in any other iron-based superconductors [4,5]. We analyze this transition in more detail by determining the flux quantum Φ_0 and intervortex spacing L in Figs. 2(b) and 2(c), respectively. Using these parameters, we estimate the lattice form factor $\sigma = L^2 B / \Phi_0$ [Fig. 2(d)] and can quantitatively track the geometrical transition of the reordering through the largest angle α between the neighboring vortex Bragg spots [Fig. 2(c)] (from 60° to 90°) and σ (from 0.86 to 1). A

striking observation is that $L \sim 5.7\xi$ ($\xi = 4.5$ nm) at approximate transition field 3 T, indicating that the wave functions of the vortex core states (diameter of $5 \sim 6\xi$) just begin to overlap at the transition. Indeed, measuring the tunneling spectra $G(V)$ far from vortex cores [Fig. 2(e)] finds that the zero-energy value G_0 becomes markedly nonzero at $B \sim 3$ T and continues to rise with increasing field [Fig. 2(f)]. Put together, the systematic behavior found in this set of data consistently suggests a scenario where the onset of overlapping vortex cores drives the transition.

While the observed overlap of the core states near 3 T in our data suggests that the vortex transition is intimately related with the intercore interaction of their anisotropic quasiparticle states, the anisotropy of the penetration depth λ (a scale set by H_{C1}) may also play a role. In order to investigate this possibility and explore the vortex anisotropy in three dimensions, we use a 2 T vector field to generate magnetic flux (Fig. 3(a); Refs. [15–18]). At various tilt angles, the far-away spectra $G(V)$ are all stateless around zero energy [Fig. 3(b)], suggesting the diminished overlap between the
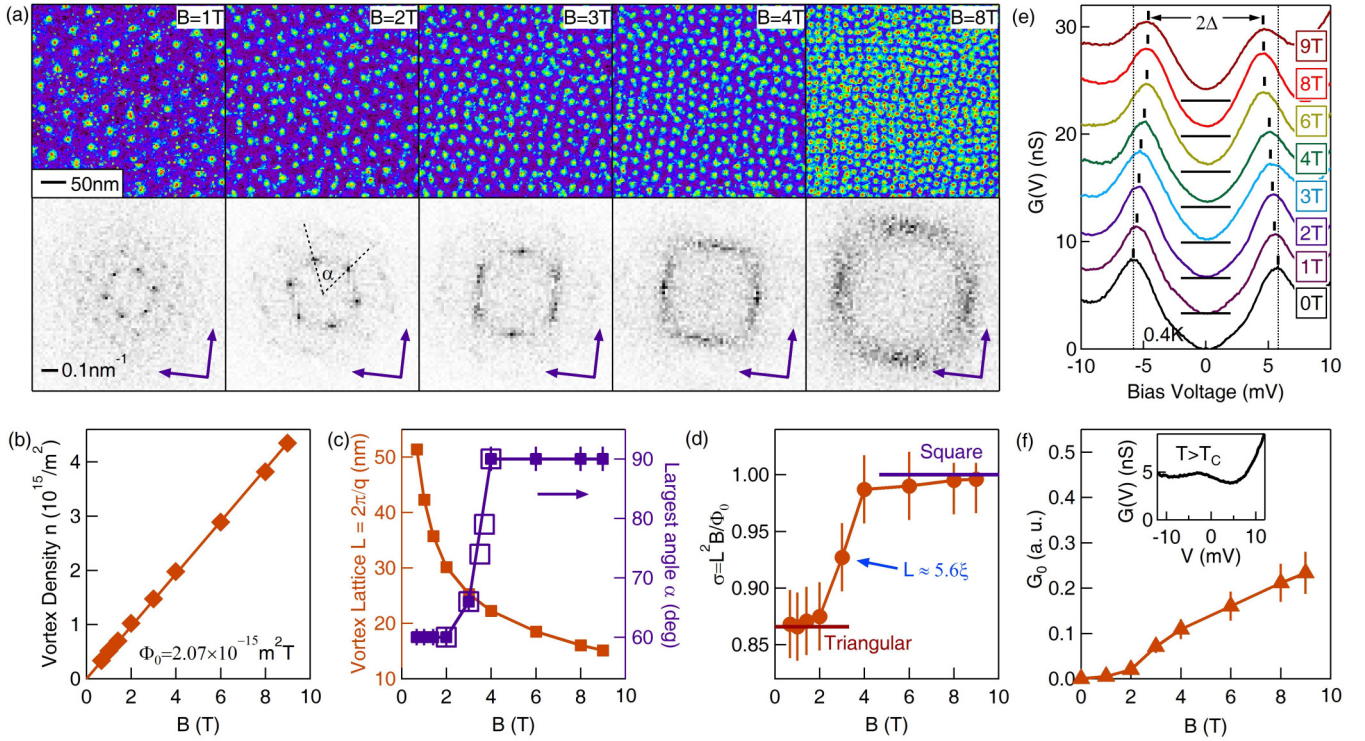
FIG. 2. (a) The upper panels are zero-energy conductance maps with varying B fields. The lower panels show their corresponding FFT image. The blue arrows illustrate the Fe-Fe (100) direction. (b) The vortex density n as a function of B, from which the flux quantum $\Phi_0 = B/n$ can be deduced. (c) The vortex lattice spacing L and the largest angle between the vortex Bragg spots α as a function of B field, respectively. (d) Field evolution of the vortex lattice form factor $\sigma = L^2 B/\Phi_0$. (e) Tunneling spectra taken away from vortex cores at different B fields (in the middle of three/four neighboring vortices). Spectra are offset for clarity. The horizontal bars mark the offset zero values. The vertical bars mark the coherent peak positions, from where we define the gap size at each field. (f) Zero-energy conductance of the spectra in (e). They are normalized by the zero-energy value in the normal state (inset image). Both the observed overlap of vortices at $L \sim 5.6\xi$ and significantly nonzero G_0 near $B = 3$ T suggest a close correlation between the intercore vortex interaction and the observed phase transition.

vortex core states. As the field is tilted towards the Fe-Fe direction ($\varphi = 0°$), the observed vortex lattice is expected to elongate along this direction. Interestingly, it remains hexagonal even at $\theta = 45°$ (also at $30°$, not plotted) and exhibits small distortions that are still weaker than expected at larger tilt angles such as $\theta = 60°$ and $\theta = 70°$ [Fig. 3(c)]. Similar distortions are observed for $\varphi = 45°$ with the elongation along the Fe-As direction [Fig. 3(d)]. A comparison of their respective Q-space-ring areas (defined as the heuristic fit to the array of vortex Bragg spots) to those of the hexagonal vortex lattices induced by c-axis fields of $B = 2T \cos \theta$ [Fig. 3(e)] shows reasonable agreement [Fig. 3(f)], indicating the internal consistency of our experimental systematics. Since the magnetic flux should be parallel to the field vector [Fig. 3(a)], the observed weak distortions even at high tilt angles combined with the internal data consistency point to a strong intrinsic vortex lattice anisotropy. This is shown in the inset of Fig. 3(g) by projecting the Q-space rings ($\varphi = 0°$) to the field normal plane [15,16]. In this view, the projected Q-space ring exhibits progressive elliptical distortions with increasing tilt angle, which can be characterized by the factor $\gamma = $ (semimajor axis/semiminor axis)$^{0.5}$ plotted in Fig. 3(g). The anisotropic London or Landau-Ginzburg theories [19] predict such elliptical distorted vortices to be generated due to anisotropy in the penetration depth or effective mass (as $\lambda \propto m^{0.5}$) with $\gamma = (1 + m_{ab}/m_c \tan^2\theta)^{-1/4}\cos^{-1/2}\theta$. Fitting

with such theory gives $m_{ab}/m_c = 0.11$ for both $\varphi = 0°$ and $\varphi = 45°$ [Fig. 3(g)]. The same magnitude of anisotropy for both φ directions suggests that $\lambda_{abFe-Fe} \approx \lambda_{abFe-As}$ or, at the very least, that the in-plane anisotropy of the penetration depth has little effect on the vortex lattice.

As the data collectively indicates the onset of a vortex core overlap scenario, it is meaningful to further investigate the relationship between Cooper pairing and the observed vortex many-body behavior. As magnetic flux explicitly breaks time-reversal symmetry, it can induce scattering processes that break Cooper pairs into decoupled quasiparticles. In our data, we observe larger tunneling intensity associated with the vortex core state along the Fe-As (110) direction (Fig. 4(a); Ref. [11]). This is clearly indicative of larger magnitude pair-breaking processes when Cooper pairs carry momentum along this direction. With increasing field, the growing overlap of the vortex core states leads to a transition to a squarelike lattice [Fig. 2 and Fig. 4(b)]. Since the zero-energy autocorrelation and FFT analysis give a measure of the elastic scattering associated with the vortex lattice, we can gain insights into the global effect of pair breaking. The data [Fig. 2 and Fig. 4(b)] suggest that the vortex lattice appears to transform in a way that minimizes the quasiparticle scattering along the Fe-As direction along which the pair-breaking effect is expected to be stronger, as discussed above for Fig. 4(a). One can gain further insight by considering the variation of the
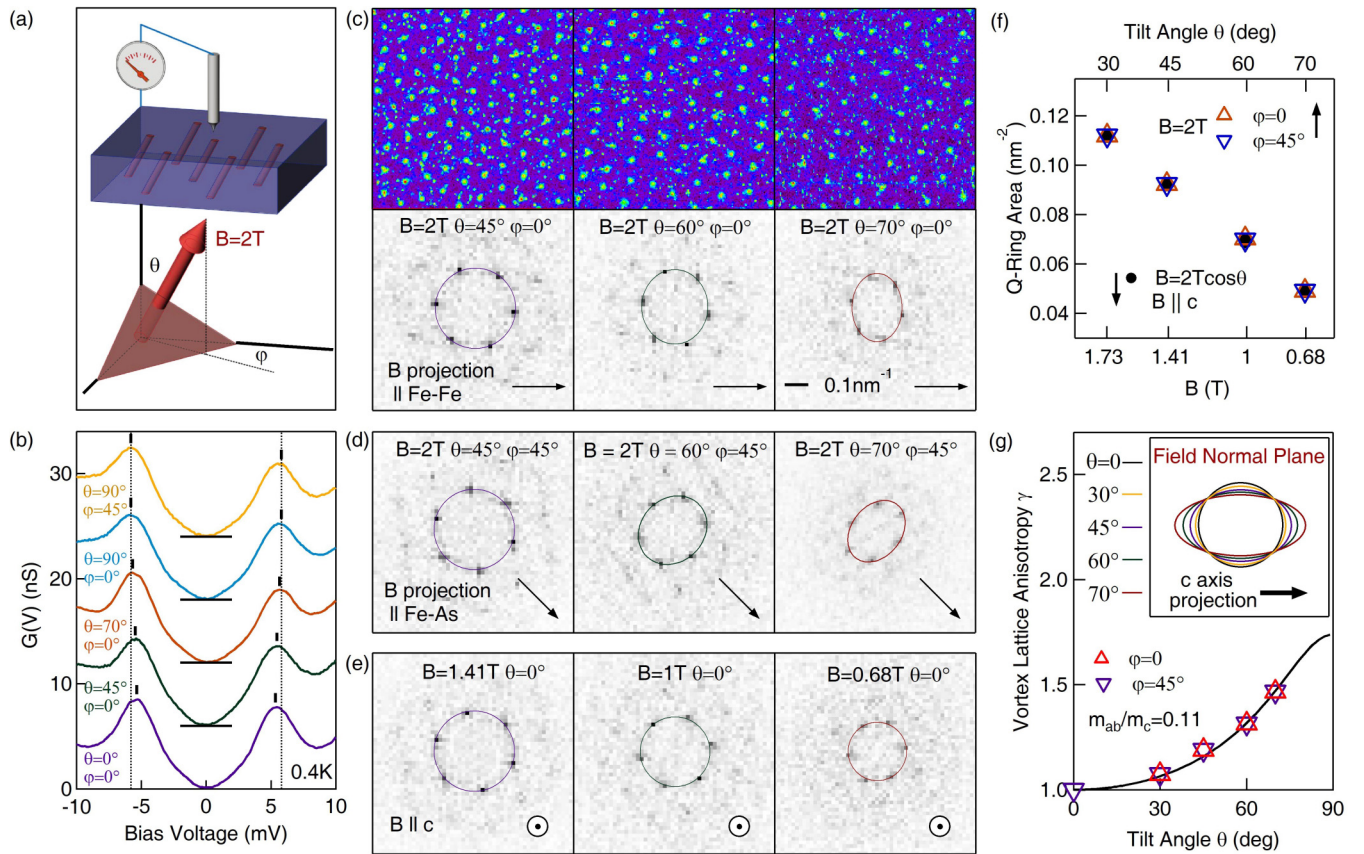
FIG. 3. (a) Geometric relationship between the applied field and the sample surface: 2 T vector field (red arrow), plane normal to field (light red surface), the induced vortex flux (purple tubes) in the crystal (blue box) and the STM tip (gray). (b) Tunneling spectra taken away from vortex cores. (c) The upper panels are zero-energy conductance maps for an area of 400×400 nm with the 2 T field tilting toward the Fe-Fe direction. The lower panels show their corresponding FFT images, and the elliptical rings are the heuristic fits to the array of Bragg peaks. (d) FFT images of data measured with the field tilting toward the Fe-As direction. (e) FFT images of data measured with the fields applied along the c axis with a magnitude of $2T\cos\theta$. (f) Comparison of the Q-space-ring area observed with tilted fields and c-axis fields. (g) The inset image plots the Q-space ring projected in the field normal plane, which mimics the intrinsic vortex lattice anisotropy consistent with the data. The main panel plots the anisotropy factor γ and a fit to theory.

superconducting gap magnitude as a function of the varying c-axis field that we control [Fig. 4(d)]. In fact, the gap reduction rate becomes notably smaller when the field is raised above 3 T. These observations collectively support the view that the global impact of the pair breaking is partially weakened upon the vortex lattice phase transition.

In order to probe the anisotropic nature of magnetic flux scattering and its correlation with the superconducting gap magnitude, we systematically tune the field from a vertical towards a horizontal configuration. We observe that a tilted 2 T field distorts the vortex lattice elliptically due to effective mass anisotropy [Fig. 3 and Fig. 4(c)]. While the vortex density remains constant, the gap size progressively recovers to the original value as the field tilts towards the in-plane directions [Fig. 4(e)]. The gap recovery is consistent with the upper critical field anisotropy and underlines that the 2 T in-plane field has a negligible effect on the superconducting gap structure. In order to further understand this c-axis field-induced pair-breaking scattering from a band structure point of view, we measure the field-dependent Bogoliubov quasiparticle interference (QPI) (Figs. 4(f) and 4(g); and

Supplemental Material [20]). From the differential QPI between the 2 T c-axis field and 0 T [Figs. 4(h) and 4(i)], we identify two scattering vectors where field-induced scattering is enhanced: $Q1 = (\pi, \pi)$ (interelectron pockets in the one-iron Brillouin zone) and $|Q2| \sim 0.3\pi$ (interhole-pocket scattering). The QPI signals at other vectors are either weakly enhanced or decreased [Fig. 4(i)]. This can be attributed to the Doppler shift of QP energies and possible sign reversal of the superconducting gaps known to occur in other superconductors [21]. Our observation of these enhanced magnetic scattering vectors is consistent with an $S\pm$ pairing symmetry [22]. We further note in our data that while $Q2$ is almost isotropic, $Q1$ is along the Fe-As direction, coincident with the stronger pair-breaking direction.

The superconducting gap magnitude characterizes the strength of Cooper pairing, while the Bogoliubov QPI signal is determined by the symmetry of Cooper pairing, and they are demonstrated here to be either correlated with the vortex transition or vortex anisotropy. Thus, there exists a strong experimental link between vortex lattice symmetry and intrinsic superconducting properties (Cooper pairing) of this material.
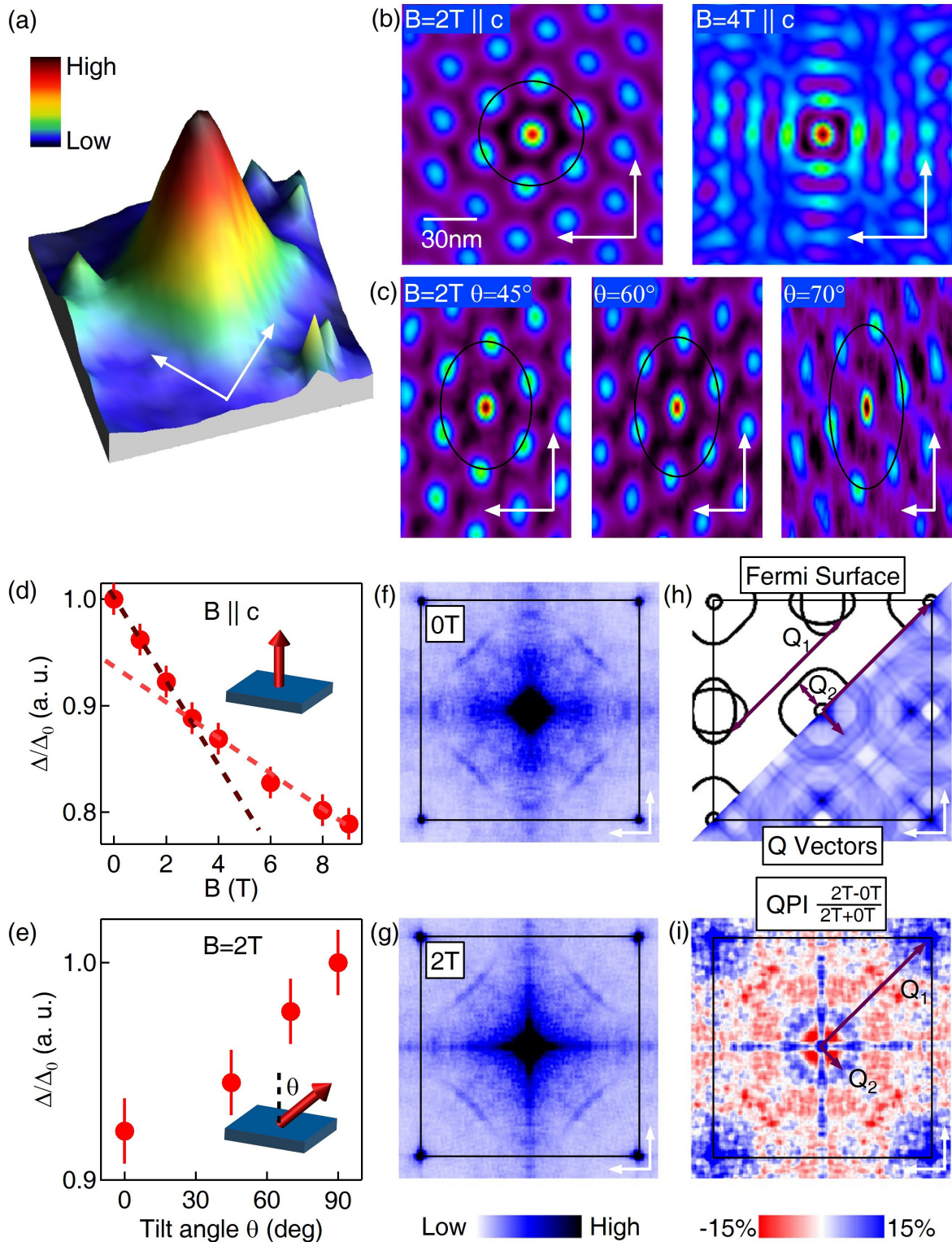
FIG. 4. (a) Three-dimensional plot of the anisotropic vortex core state (17×17 nm). The white arrows indicate the Fe-Fe real-space directions. (b) Autocorrelation image of the vortex lattice data for c-axis fields $B = 2$ T and $B = 4$ T, respectively, revealing the vortex transition. (c) Projected autocorrelation images of the vortex lattice data for tilted 2 T B fields ($\varphi = 0$), showing the intrinsic vortex distortion observed. These images are projected to the field normal plane, so that the white arrow horizontal axis is shortened correspondingly. (d) Superconducting gap variation as a function of the c-axis field [extracted from the data in Fig. 2(e)]. (e) Superconducting gap variation as a function of tilt angles of a 2 T vector field [extracted from data in Fig. 3(b)]. (f),(g) QPI data taken at -5 meV around the same area with zero field and a 2 T c-axis field, respectively. The black frame corresponds to one-iron Brillouin zone. (h) Schematic of the Fermi surface and simulation of all possible scattering Q vectors. (i) Normalized differential QPI signal between 2 T (c axis) and 0 T.

Moreover, as can be seen in Fig. 4(h), the outer Fermi surfaces are squarelike, and the multiband effects associated anisotropy in the Fermi velocity can contribute to the vortex anisotropy and its transition [22–33]. Unlike the vortex transition in borocarbides [31,32] and V_3Si [33] that can be described by the nonlocal corrections to the London model (Ref. [28], valid for weakly coupled anisotropic superconductors with small κ), LiFeAs is a multiband, large $\kappa(\approx 50)$, strong-coupling superconductor with sign reversal in the superconducting order parameter. A quantitative understanding of the vortex lattice evolution and its connection to the superconducting gap variations and Bogoliubov quasiparticle scattering in our experiments thus requires a comprehensive quantum many-body theory which takes its multiband nature and unconventional Cooper pairing into account. Crucially, we have visualized rich vortex lattice symmetries and their interplay with the Cooper pairing in a single material, which is a clear experimental advance in the vector magnetic field study of correlated superconductors. Finally, we note that the vortex lattice tunability and the vector field based spectroscopic imaging we demonstrated here can also contribute to the development of future technological advances and applications [34–36].

[1] B. Keimer and J. E. Moore, Nat. Phys. **13**, 1045 (2017).

[2] E. Fradkin, S. A. Kivelson, and J. M. Tranquada, Rev. Mod. Phys. **87**, 457 (2015).

[3] Ø. Fischer, M. Kugler, I. Maggio-Aprile, C. Berthod, and C. Renner, Rev. Mod. Phys. **79**, 353 (2007).

[4] J. Hoffman, Rep. Prog. Phys. **74**, 124513 (2011).

[5] G. R. Stewart, Rev. Mod. Phys. **83**, 1589 (2011).

[6] S. V. Borisenko, V. B. Zabolotnyy, D. V. Evtushinsky, T. K. Kim, I. V. Morozov, A. N. Yaresko, A. A. Kordyuk, G. Behr, A. Vasiliev, R. Follath, and B. Büchner, Phys. Rev. Lett. **105**, 067002 (2010).

[7] K. Umezawa, Y. Li, H. Miao, K. Nakayama, Z.-H. Liu, P. Richard, T. Sato, J. B. He, D.-M. Wang, G. F. Chen, H. Ding, T. Takahashi, and S.-C. Wang, Phys. Rev. Lett. **108**, 037002 (2012).

[8] M. P. Allan, A. W. Rost, A. P. Mackenzie, X. Yang, J. C. Davis, K. Kihou, C. H. Lee, A. Iyo, H. Eisaki, and T.-M. Chuang, Science **336**, 563 (2012).

[9] Shun Chi, S. Grothe, Ruixing Liang, P. Dosanjh, W. N. Hardy, S. A. Burke, D. A. Bonn, and Y. Pennec, Phys. Rev. Lett. **109**, 087002 (2012).

[10] N. Kurita, K. Kitagawa, K. Matsubayashi, A. Kismarahardja, E-S Choi, J. S. Brooks, Y. Uwatoko, S. Uji, and T. Terashima, J. Phys. Soc. Jpn. **80**, 013706 (2011).

[11] T. Hanaguri, K. Kitagawa, K. Matsubayashi, Y. Mazaki, Y. Uwatoko, and H. Takagi, Phys. Rev. B **85**, 214505 (2012).

[12] J. Ferber, K. Foyevtsova, R. Valenti, and H. O. Jeschke, Phys. Rev. B **85**, 094505 (2012).

[13] D. S. Inosov, J. S. White, D. V. Evtushinsky, I. V. Morozov, A. Cameron, U. Stockert, V. B. Zabolotnyy, T. K. Kim, A. A. Kordyuk, S. V. Borisenko, E. M. Forgan, R. Klingeler, J. T. Park, S. Wurmehl, A. N. Vasiliev, G. Behr, C. D. Dewhurst, and V. Hinkov, Phys. Rev. Lett. **104**, 187001 (2010).

[14] X. S. Ling, S. R. Park, B. A. McClain, S. M. Choi, D. C. Dender, and J. W. Lynn, Phys. Rev. Lett. **86**, 712 (2001).

[15] H. F. Hess, C. A. Murray, and J. V. Waszczak, Phys. Rev. B **50**, 16528 (1994).

[16] H. F. Hess, C. A. Murray, and J. V. Waszczak, Phys. Rev. Lett. **69**, 2138 (1992).

[17] S. J. Kuhn, W. Morgenlander, E. R. Louden, C. Rastovski, W. J. Gannon, H. Takatsu, D. C. Peets, Y. Maeno, C. D. Dewhurst, J. Gavilano, and M. R. Eskildsen, Phys. Rev. B **96**, 174507 (2017).

[18] P. Das, J. S. White, A. T. Holmes, S. Gerber, E. M. Forgan, A. D. Bianchi, M. Kenzelmann, M. Zolliker, J. L. Gavilano, E. D. Bauer, J. L. Sarrao, C. Petrovic, and M. R. Eskildsen, Phys. Rev. Lett. **108**, 087002 (2012).

[19] K. G. Petzinger and G. A. Warren, Phys. Rev. B **42**, 2023 (1990).

[20] See Supplemental Material at http://link.aps.org/supplemental/10.1103/PhysRevB.99.161103 for systematic QPI data and analysis.

[21] T. Hanaguri, S. Niitaka, K. Kuroki, and H. Takagi, Science **328**, 474 (2010).

[22] P. J. Hirschfeld, M. M. Korshunov, and I. I. Mazin, Rep. Prog. Phys. **74**, 124508 (2011).

[23] Y. Gao, H-X. Huang, C. Chen, C. S. Ting, and W-P. Su, Phys. Rev. Lett. **106**, 027004 (2011).

[24] Y. Wang, P. J. Hirschfeld, and I. Vekhter, Phys. Rev. B **85**, 020506(R) (2012).

[25] K. Lee, M. H. Fischer, and E-A Kim, New J. Phys. **15**, 053048 (2013).

[26] B. M. Uranga, M. N. Gastiasoro, and B. M. Andersen, Phys. Rev. B **93**, 224503 (2016).

[27] K. Takanaka, Prog. Theor. Phys. **46**, 1301 (1971).

[28] V. G. Kogan, M. Bullock, B. Harmon, P. Miranovic, L. Dobrosavljevic-Grujic, P. L. Gammel, and D. J. Bishop, Phys. Rev. B **55**, R8693(R) (1997).

[29] M. Ichioka, A. Hasegawa, and K. Machida, Phys. Rev. B **59**, 8902 (1999).

[30] B. Keimer, W. Y. Shih, R. W. Erwin, J. W. Lynn, F. Dogan, and I. A. Aksay, Phys. Rev. Lett. **73**, 3459 (1994).

[31] H. Sakata, M. Oosawa, K. Matsuba, N. Nishida, H. Takeya, and K. Hirata, Phys. Rev. Lett. **84**, 1583 (2000).

[32] U. Yaron, P. L. Gammel, A. P. Ramirez, D. A. Huse, D. J. Bishop, A. I. Goldman, C. Stassis, P. C. Canfield, K. Mortensen and M. R. Eskildsen. Nature (London) **382**, 236 (1996).

[33] C. E. Sosolik, Joseph A. Stroscio, M. D. Stiles, E. W. Hudson, S. R. Blankenship, A. P. Fein, and R. J. Celotta. Phys. Rev. B **68**, 140503(R) (2003).

[34] J.-X. Yin, S. S. Zhang, H. Li, K. Jiang, G. Chang, B. Zhang, B. Lian, C. Xiang, I. Belopolski, H. Zheng, T. A. Cochran, S.-Y. Xu, G. Bian, K. Liu, T.-R. Chang, H. Lin, Z.-Y. Lu, Z.

Wang, S. Jia, W. Wang, and M. Zahid Hasan, Nature (London) **562**, 91 (2018).

[35] J.-X. Yin, S. S. Zhang, G. Chang, Q. Wang, S. S. Tsirkin, Z. Guguchia, B. Lian, H. Zhou, K. Jiang, I. Belopolski, N. Shumiya, D. Multer, M. Litskevich, T. A. Cochran, H. Lin, Z. Wang, T. Neupert, S. Jia, H. Lei, and M. Zahid Hasan, Nat. Phys. (2019), doi:10.1038/s41567-019-0426-7.

[36] H. Zheng and M. Zahid Hasan, Adv. Phys.: X **3**, 1466661 (2018).